CHAPTER 3
INTERACTION OF PRISTINE AND DEFECTED α-CX (X = N, P) MONOLAYERS WITH TOXIC GASES

3.1. INTRODUCTION

In Chapter 1, the thesis emphasized the serious health hazards posed by dangerous gases such as carbon monoxide (CO) and nitrogen oxide (NO). These gases, frequently emitted from the improper combustion of fossil fuels, represent significant threats to both the environment and human health.[1] CO and NO are particularly perilous because they are colorless and odorless, which can lead to fatalities due to unconsciousness or severe respiratory problems upon exposure. Due to these risks, there has been a significant increase in the demand for gas detection technologies. This has led to extensive research into different two-dimensional materials such as graphene, hexagonal boron nitride (h-BN), hexagonal aluminium carbide (h-AlC), graphitic carbon nitride (g-C_3N_4) etc. Numerous studies have examined the gas adsorption behaviours of two-dimensional materials of their interactions with different hazardous gases. These investigations highlight the potential for developing highly sensitive and responsive gas sensors[2,3,4]. Despite these advancements, the current chapter focuses on the largely untapped potential of dynamically stable Group IV and V atoms based α-CX (X=N and P) monolayers for gas sensing applications. Prior research has explored the structural and electronic properties of these monolayers revealing its unique semiconductor characteristics and its potential use in UV light and photo detection, water splitting reaction, and energy storage application[5,6,7]. However, studies on its gas adsorption performance, particularly with hazardous gases such as CO and NO are still limited.

As per the results and discussion, pristine α-CX (X = N, P) monolayers are inadequate for CO and NO sensing due to their low adsorption energy and large adsorption distances[8]. A study was conducted by Ahuja et al. and collaborators, focusing on the electronic response of both pristine and defected 2D h-BN to NO molecules using DFT calculations[2]. The findings revealed a weak interaction between NO and bare h-BN, while mono-vacancy defects enhance the reactivity between them. In same direction, Zhang et al. also conducted a study to evaluate the interactions between various pollutants, such as CO, NO, NO_2 and NH_3, with four different states of graphene: pristine, defective, B doped and N doped, to reveal their potential applications as pollutant sensor[9]. Pristine 2D phosphorene is not reliable for CO and NO sensing, but its defective form excels as a sensor for both gas molecules[10]. Also, a study by Yawen Gao et al suggested that S defected MoS_2 is more suitable for CH_2O sensing[11]. Taking into account the existing literature, we have introduced a vacancy defect by removing one carbon atom for the augmentation of the adsorption performance α-CX (X = N, P) of pristine monolayers.

The present chapter aims to examine the sensing performance of C defected α-CX (X = N, P) monolayers towards CO and NO gases compared to the pristine α-CX (X = N, P) monolayers. The findings of this chapter will be useful not only in synthesizing low-cost, very sensitive sensors for detecting hazardous gases but also in understanding how these systems interact on the surface with said gases.

3.2. COMPUTATIONAL DETAILS

For all the calculations of structural and electronic properties of α- CX (X=N and P), ab-initio DFT calculations[12] were executed using Quantum Espresso package.[13] Generalized gradient approximation-based pseudo potentials,[14] proposed by Perdew-Burke-Ernzerhof were considered for exchange-correlation interaction. The electronic wave functions were expanded with a plane wave basis set, utilizing cut-off energies of 70 Ry and a charge density cutoff of 280 Ry. To minimize the interaction between successive monolayers, a 20 Å vacuum slab was inserted in the Z direction. The Brillouin zone integration was sampled with a 7×7×1 K-mesh grid constructed under the Monkhorst-Pack scheme. [15]Van der Waals corrections, as Grimme's DFT-D2, were considered to describe the interaction between adsorbed gases and the α-CX (X = N and P) sheet. The Marzari-Vanderbilt smearing was applied for the necessary calculations. An iterative convergence process was employed to obtain the relaxed configuration for each structure, continuing until the maximum Hellmann-Feynman force on each atom was below 10^{-3} eV/Å. 3×3×1 supercell of α-CX (X = N and P) containing 36 atoms was used to investigate the adsorption properties. The adsorption energy was calculated using the following equation[16]:

$$E_{ads} = E_{system+gas} - (E_{system} + E_{gas}) \text{ ---- (1)}$$

Where, $E_{(system+gas)}$ is the total energy of α- CX (X=N and P) with gas adsorbed on it, E_{system} is the energy of 2D α-CX (X=N and P) and E_{gas} is the energy of CO and NO gas molecules. Negative value of adsorption energy indicates that the process is exothermic, and the gas molecules can adsorb stably on the monolayer system.

3.3 RESULT AND DISCUSSION

3.3.1. Structural and electronic properties of pristine and defect tuned α-CX (X = N and P) monolayers

α-CN and α-CP possess hexagonal crystal structure with $P\bar{6}m2$ symmetry. Figure 3.1 shows the top and side views of the optimized crystal structures of α-CX (X= N and P). In the case of α-CN observed bond lengths are 1.63, 2.64, 1.45 Å between carbon-carbon (C-C), nitrogen-nitrogen(N-N), and carbon-nitrogen (C-N) and observed angles are 110.1° and 108.7° between carbon-carbon-nitrogen (C-C-N) and nitrogen-carbon-nitrogen(N-C-N) respectively. (See Table 3.1) The observed bond lengths in case of α-CP are 1.55, 3.29, 1.88 Å between carbon-carbon (C-C), phosphorous- phosphorous (P-P) and carbon-phosphorous (C-P), while in the same the angles along carbon-carbon-phosphorous (C-C-P) and phosphorous-carbon-phosphorous (P-C-P) pairs are found to be 117.6° and 100.1°. The optimized lattice parameters of α-CN and α-CP are 2.368 and 2.881 Å, respectively which are in agreement with the previously reported data[6]. There is an indirect band gap of 3.77 eV in pristine α-CN and direct band gap of 1.78 eV in pristine α-CP which clearly shows that both systems are semiconducting [see Fig. 3.1 (b) and (e)]. Plotted projected density of states (PDOS) of both optimized structures are shown in figure 3.1 (c) and (f). Apparently for α-CN, in the formation of VBM (valance band maxima), the contribution of N-2p orbital is more and in the formation of CBM (conduction band minima), the contribution of C-2p orbitals is more. Moreover, in α-CP, C-2p orbital give more contribution for the formation of VBM and P-3p orbital give more contribution in the formation of CBM.

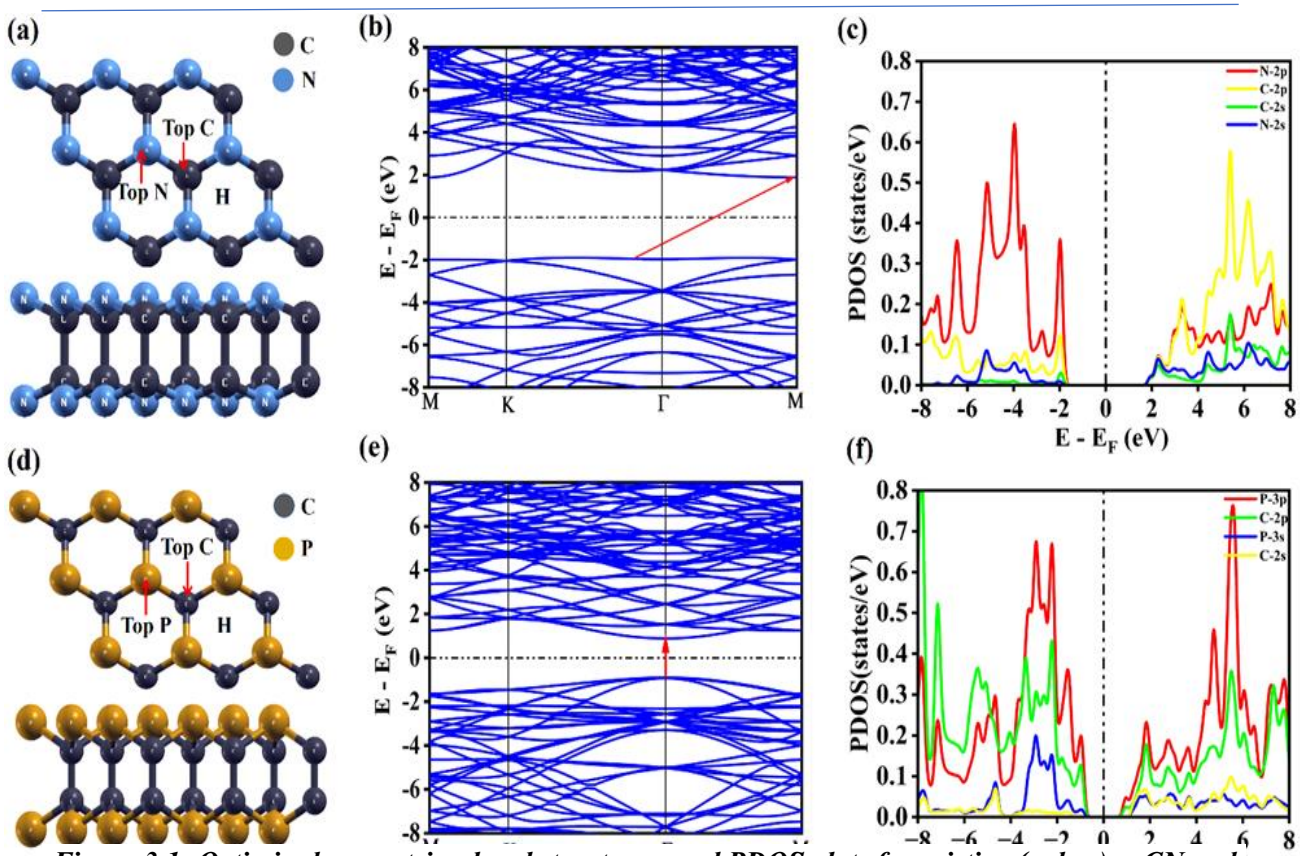

Figure 3.1: Optimized geometries, band structures, and PDOS plots for pristine (a, b, c) α-CN and (d, e, f) α-CP monolayers, respectively

For defect-tuning, a vacancy was introduced by removing a carbon atom from pristine α-CX (X= N and P) monolayers. The optimized structures of α-CN and α-CP with a carbon defect are depicted in Fig. 3.2(a) and (d). The introduction of this defect leads to structural alterations, and both systems transform into extrinsic semiconductors with change in the energy band gap values, as shown in Fig. 3.2 (b) and (e)

Table 3.1 Comparison of lattice parameters, bond lengths, angles, and electronic band gaps for pristine and C-defected α-CX (X = N, P) monolayers

Mono layer	System	Lattice (Å)	Bond length (Å)			Angle (º)		E_g (eV)	Ref.
			C-C	X-X	C-X	θ_1 (C-C-X)	θ_2 (C-X-C)		
α- CN	Pristine	2.37	1.63	2.64	1.46	110.21	108.73	3.77	Our work
		2.38	1.63	2.65	1.46	110.35	108.58	3.71	[17]
	C-defected	2.37	1.67	2.63	1.46	109.27	111.16	-	Our work
α- CP	Pristine	2.88	1.55	3.29	1.87	117.65	100.17	1.78	Our work
		2.90	1.55	3.29	1.88	117.50	100.39	1.82	[6]
	C-defected	2.88	1.53	3.32	1.85	121.37	100.62	-	Our work

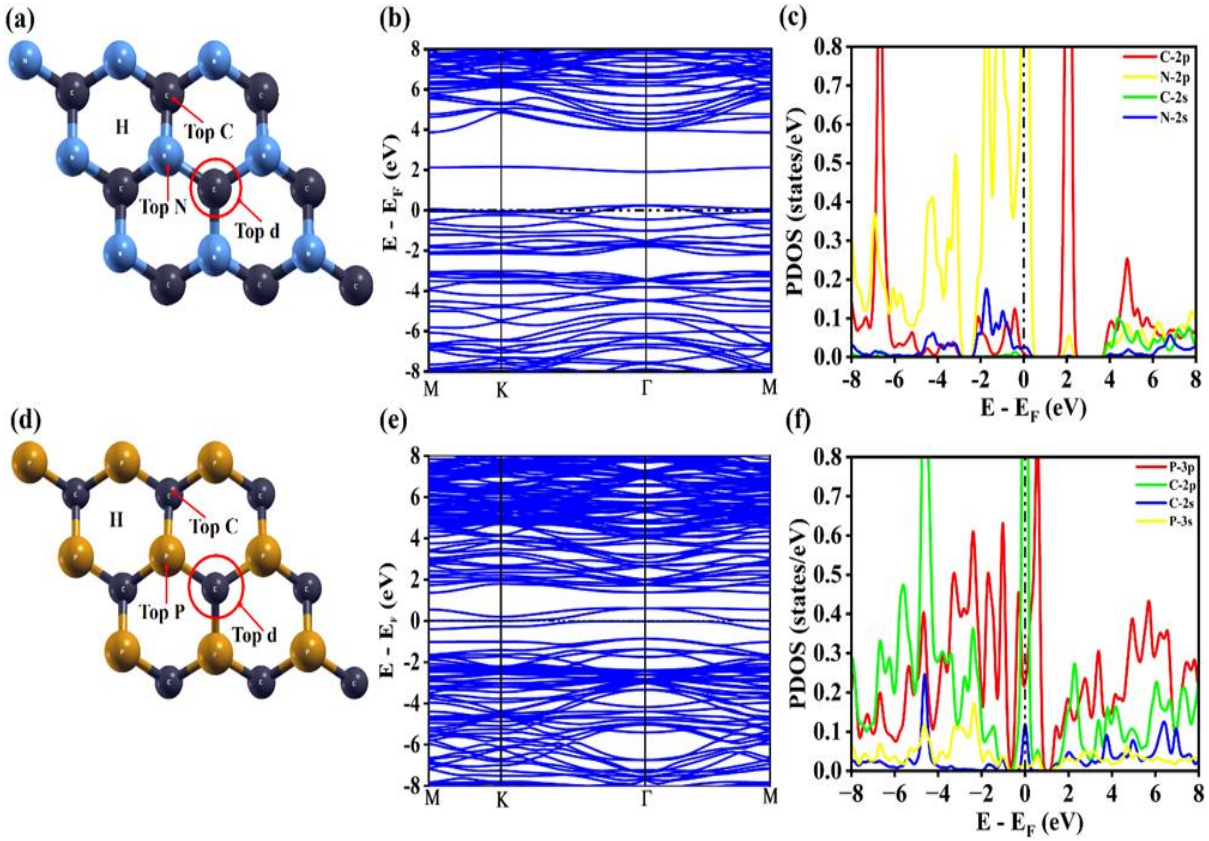

Figure 3.2 Optimized geometries, band structures, and PDOS plots for C-defected (a, b, c) α-CN and (d, e, f) α-CP monolayers, respectively

3.3.2 Adsorption performance of CO gas molecule over pristine and C defected α-CX monolayers

We have done optimization of CO gas molecule individually before the calculation of the adsorption energy of gas molecules over α-CN and α-CP monolayers. Optimized bond lengths of CO molecules 1.12 Å which validates well with the previously reported data [18]. There are three possible sites for the adsorption i.e. top of carbon, top of X (X= N, P) and on hollow sites. Among all these possible configurations for each gas molecules, we further considered only most stable configurations i.e., minimum energetic configurations. For the adsorption of CO gas molecule over α-CN and α-CP, the minimum energetic configuration is shown in fig 3.3 (a) and (d) with values of adsorption energy of -0.08 eV and -0.07 eV along with the adsorption distance of 3.11 Å and 3.91 Å. Low value of adsorption energy and larger adsorption distance indicates physisorption between the toxic gas and the system. Also, there is no visible decrement in the bandgap of the system (see fig 3.3 (b) and (e)). In the partial

density of states, there is no indication of overlapping orbitals at the Fermi level, which further reinforces the evidence for physisorption. (Fig 3.3 (c) and (f))

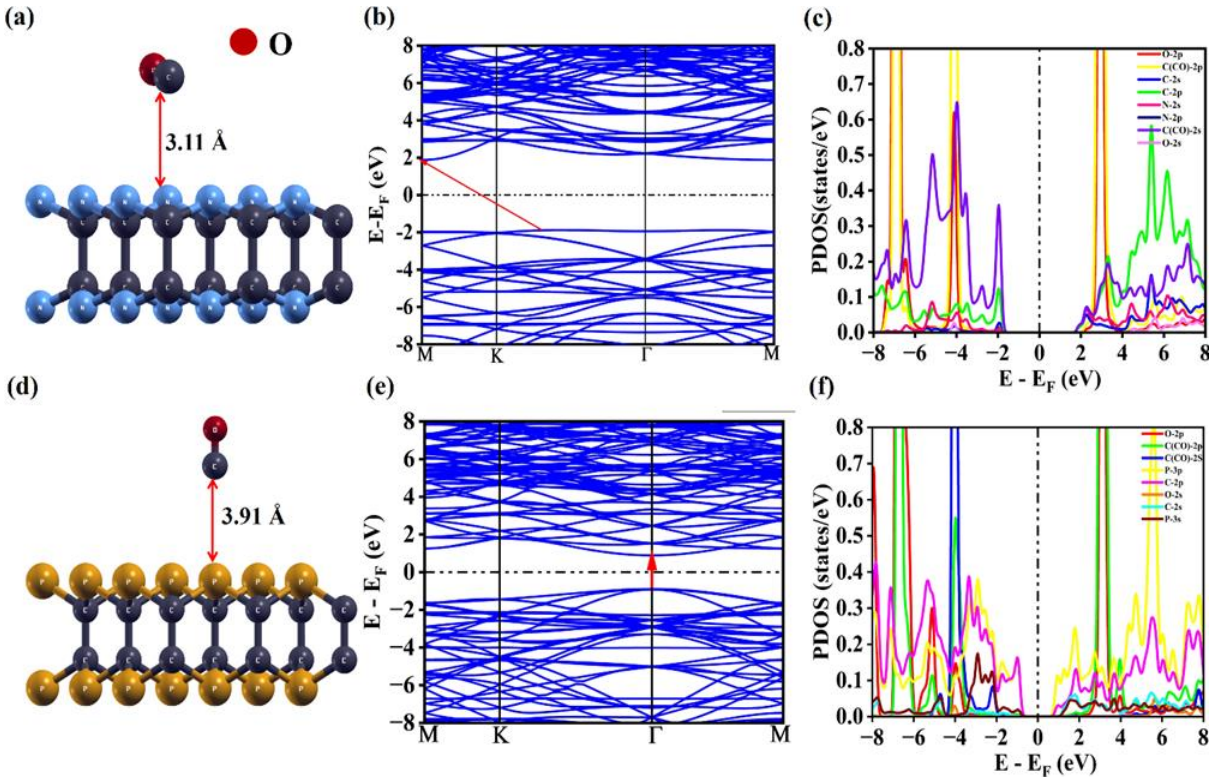

Figure 3.3: Minimum energetic configurations, band structures, and PDOS plots for CO adsorbed pristine (a, b, c) α-CN and (d, e, f) α-CP monolayers, respectively

To enhance the sensing capabilities of α-CX (X = N and P) monolayers, we have introduced a defect within the structure by removing one carbon atom. For the adsorption of CO gas molecules, four potential sites were considered: the top of the carbon atom, top of the X atom (X= N, P), top of the defect, and the hollow site. Among these configurations, the most stable configuration for α-CN is CO molecule adsorbed on top of the carbon atom, with an adsorption energy of -3.63 eV and an adsorption distance of 0.78 Å. (Table 3.2) These values indicate strong chemisorption between the CO gas molecule and the C-defected α-CN monolayer. This chemisorption transforms the semiconductor into an extrinsic type, leading to the formation of impurity states at the Fermi level.[19] Consequently, the conductivity of the extrinsic semiconductor increases as the band gap decreases from 3.78 eV to 1.80 eV (See Figure 3.4(b)). The projected density of states (PDOS) analysis reveals hybridization of p

orbitals of C(CO)-2p and N-2p, indicating qualitative charge transfer between the monolayer and the gas molecule. (Figure 3.4 (c))

For the C-defected α-CP monolayer, the most stable configuration occurs when the CO molecule is adsorbed on top of the P atom, with an adsorption energy of -1.33 eV and an adsorption distance of 1.96 Å. (See Table 3.2) Analysis of the band structure (see Figure 3.4(e)) shows that the system remains an extrinsic semiconductor after CO adsorption. However, PDOS evaluation indicates no hybridization between the electronic states of the C and O atoms in the CO molecule and the C and P atoms in the α-CP monolayer. This suggests that van der Waals forces predominantly govern the interaction between the CO gas molecule and the α-CP monolayer.

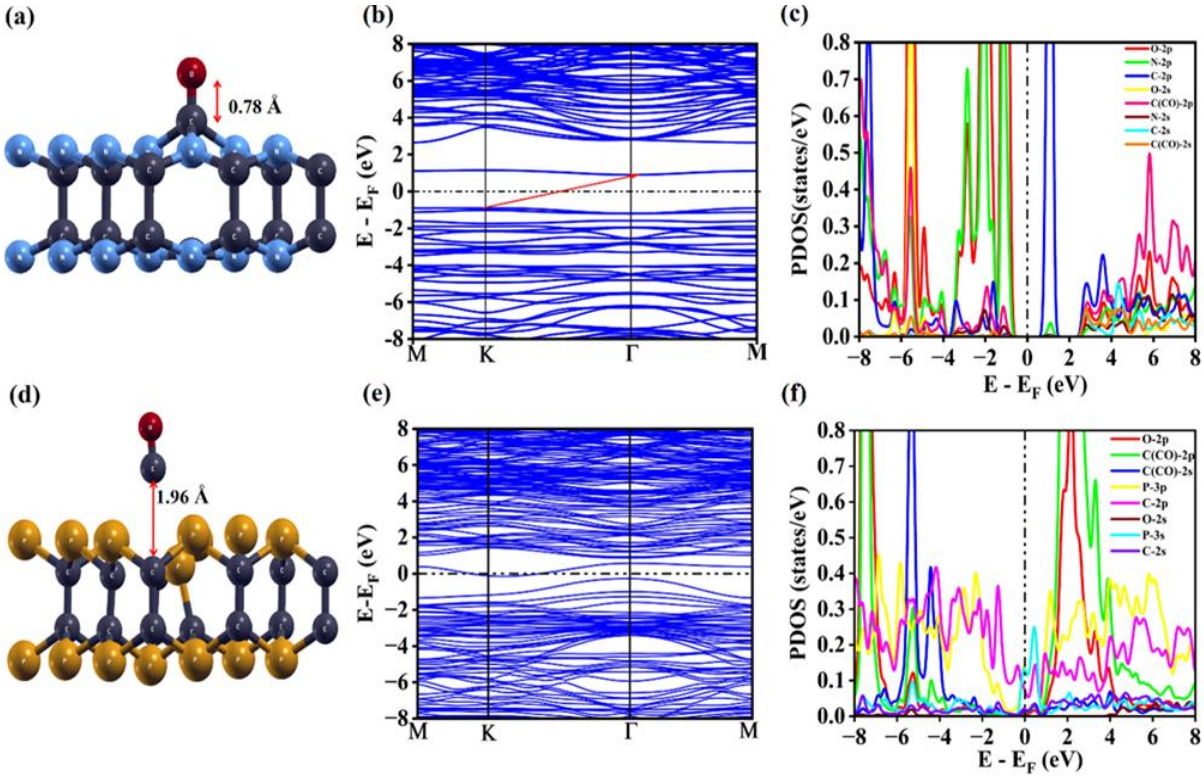

Figure 3.4: Minimum energetic configurations, band structures, and PDOS plots for CO adsorbed C-defected (a, b, c) α-CN and (d, e, f) α-CP monolayers, respectively

3.3.3 Adsorption performance of NO gas molecule over pristine and C defected α-CX monolayers

The adsorption energy of the NO molecule over the α-CN and α-CP monolayers was determined after individually optimizing the gas molecule. With an optimized bond length for NO of 1.14 Å, consistent with prior research,[18] we identified three potential sites for NO gas molecule adsorption: the top of carbon, the top of N or P, and hollow sites. Only the most stable configurations, or minimum energetic configurations, were further analysed for the gas molecule. The minimum energetic configuration for the adsorption of NO gas molecule over α-CN and α-CP is depicted in Figure 3.5 (a) and (d), showing adsorption energy values of -0.07 eV and -0.09 eV, and 3.00 Å and 3.40 Å adsorption distances, respectively. Although there is a decrease in the energy band gap value in the case of α-CP, large adsorption distance and the absence of bond formation between the system and the gas molecule indicates physisorption. between the system and the toxic gas.

For the adsorption of NO gas molecules on carbon-defected α-CN and α-CP, we have chosen the most energetically favourable configuration from the four possible sites for further studies. As discussed in section 3.2, the creation of a defect transforms both α-CN and α-CP into extrinsic semiconductors. Upon adsorption of NO gas on C defected α-CN, the system remains an extrinsic semiconductor with an adsorption energy (E_{ads}) of -1.90 eV and an adsorption distance of 1.77 Å. The most stable configuration for C defected α-CN is the NO gas adsorbed on top of the N (see Figure 3.6(a)). The overlapping of N-2p, O-2p, and C-2p orbitals at the Fermi level results in a reduced energy bandgap and increased system conductivity (see Figure 3.6(c)). For carbon-defected α-CP, among the four potential adsorption sites for the NO gas molecule, the most stable configuration is with the NO gas adsorbing on top of the carbon atom, featuring an E_{ads} of -1.98 eV and an adsorption distance of 2.16 Å. Following the adsorption of the NO gas molecule on C defected α-CP, a reduction in the energy bandgap is observed due to the overlapping of N-2p, O-2p, P-3p, C-2p, and N-2s orbitals at the Fermi level. This overlapping enhances the system's conductivity, which is a crucial characteristic for gas sensing applications.

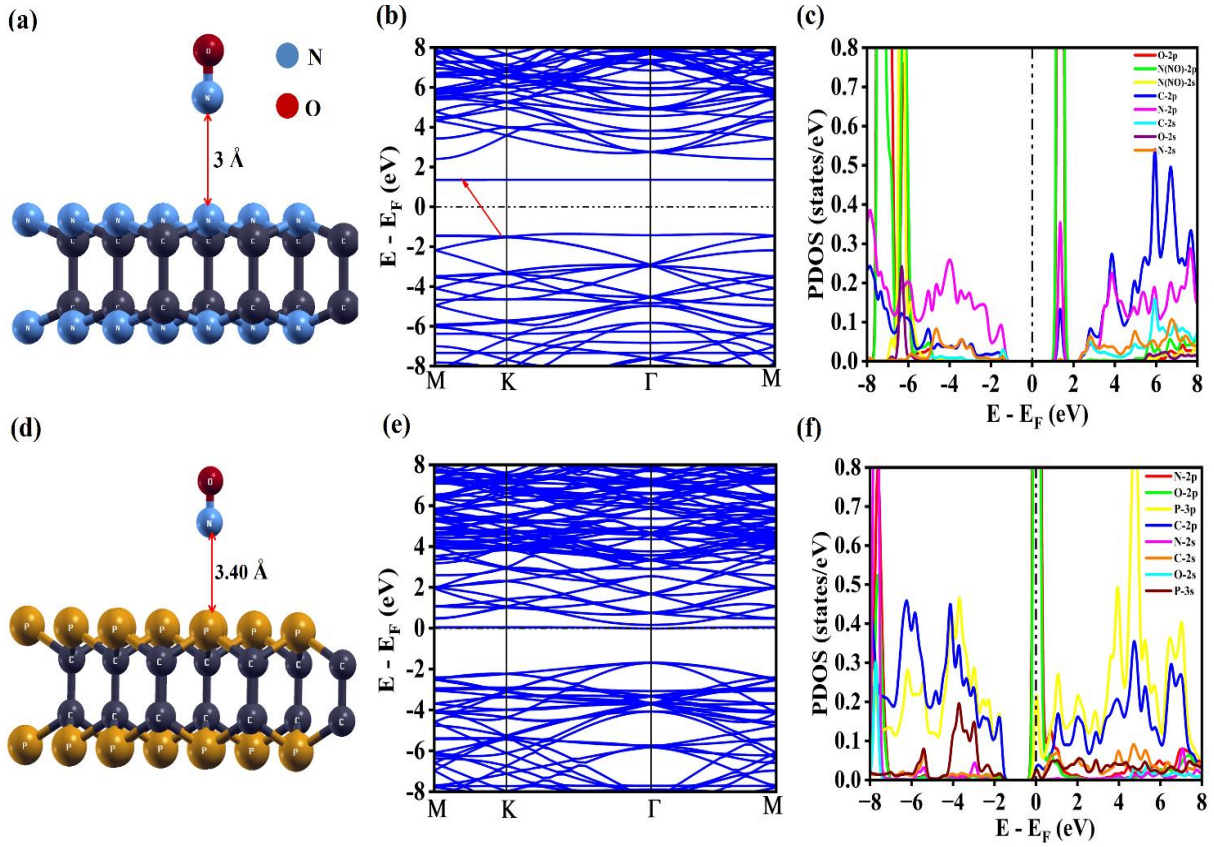

Figure 3.5: Minimum energetic configurations, band structures, and PDOS plots for NO adsorbed pristine (a, b, c) α-CN and (d, e, f) α-CP monolayers, respectively

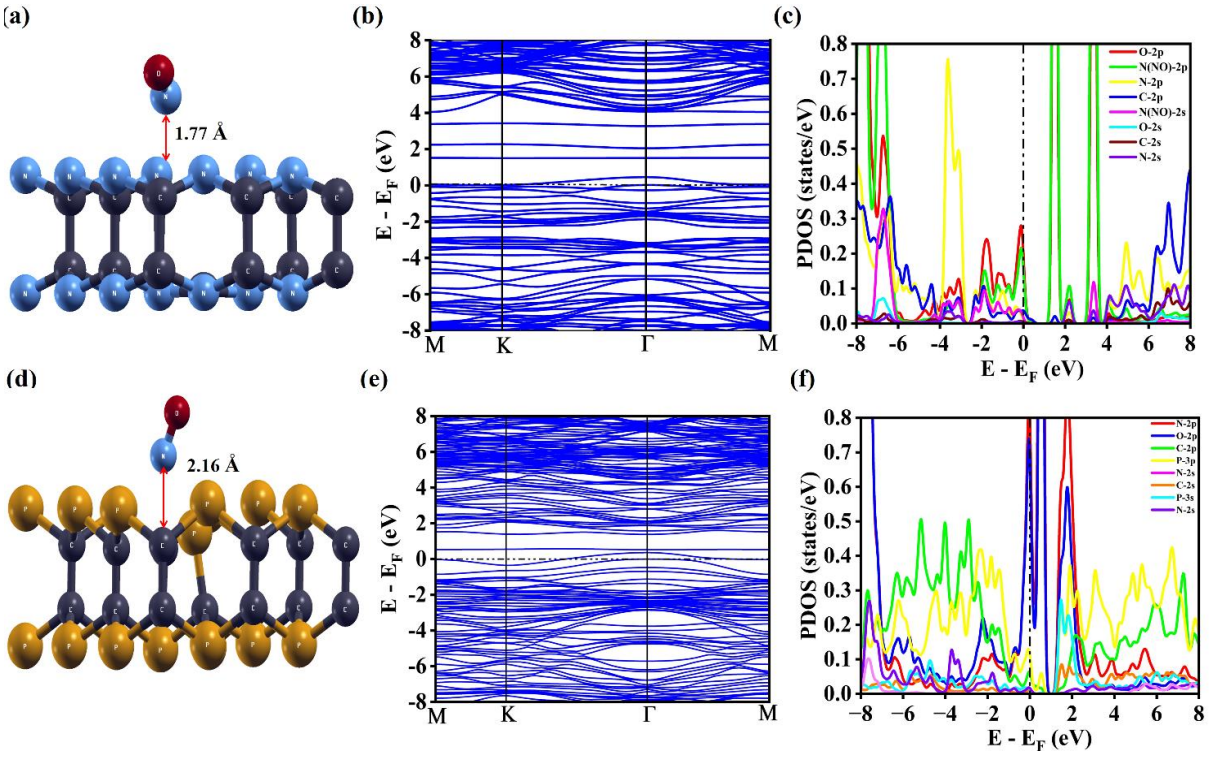

Figure 3.6: Minimum energetic configurations, band structures, and PDOS plots for NO adsorbed C-defected (a, b, c) α-CN and (d, e, f) α-CP monolayers, respectively

Table 3.2: Adsorption Energies (E_{ads}) and adsorption distances (d) for CO and NO adsorbed pristine and defected α-CX (X= N and P) monolayers, respectively.

Gas molecule	Monolayer	System	E_{ads} (eV)	d (Å)
CO	α-CN	Pristine	-0.08	3.11
		C defect	-3.63	0.78
	α-CP	Pristine	-0.06	3.91
		C defect	-1.33	1.96
		Al doped	-0.09	3.58
NO	α-CN	Pristine	-0.07	3.00
		C defect	-1.90	1.77
	α-CP	Pristine	-0.09	3.40
		C defect	-1.98	2.16

3.3.4 Charge transfer analysis

For the better understanding of interaction between α-CX (X=N, P) monolayer and gas molecule, charge transfer analysis is essential. This analysis helps quantify the strength of the interaction, tune sensing properties, and optimize material composition for enhanced sensitivity, selectivity, and specificity. For the quantitative study of charge transfer we have done Löwdin charge transfer calculation.[20]

Table 3.3 presents Löwdin charge values on gas molecules before and after the adsorption. A negative Δq value indicates that the gas exhibits charge acceptor behaviour, while a positive Δq signifies that the gas molecule behaves as a charge donor. The CO gas molecule exhibits charge donor behaviour in all instances except when adsorbed on C-defected α-CN. In contrast, the NO gas molecule functions as a charge acceptor in both pristine and defected α-CP, whereas it demonstrates charge donor behaviour in the context of both pristine and C-defected α-CN.

Table 3.3: Löwdin charge (e) analysis of pristine and defected α-CX, (X=N,P)

Gas molecule	Monolayer	System	Löwdin charge (e) on atoms	Δq(e)
CO	α-CN	Isolated gas molecule	9.9017	-
		Pristine	9.7918	0.1099
		C defect	10.0067	-0.105
	α-CP	Pristine	7.8533	2.0484
		C defect	9.9833	0.0816
NO	α-CN	Isolated gas molecule	10.916	-
		Pristine	10.4597	0.4563
		C defect	10.4866	0.4294
	α-CP	Pristine	10.988	-0.072
		C defect	11.3814	-0.4654

We have also done plotting of charge density difference for additional analysis.(Figure 3.7)

The charge density difference is evaluated by the following formula[21]:

$$\Delta\rho = \rho_{system+gas} - (\rho_{system} + \rho_{gas}) \text{ ---- } (2)$$

Where, $\rho_{system+gas}$ represents the charge density of a combined α-CX (X=N, P) monolayer with adsorbed gas system. ρ_{system} and ρ_{gas} are the total charge densities of the α-CX (X=N, P) monolayer and free gas molecule.

As per the figures, yellow colour shows charge depletion region and cyan colour shows charge accumulation region. In the case of CO gas adsorption on C defected α-CN, CO gas molecule act as a charge acceptor with creating charge depletion region on the α-CN monolayer. (figure 3.7 (a) and (b)). For CO gas adsorbed over C defected α-CP, CO gas being charge acceptor, leaves electron depletion region on a monolayer. (See figure 3.7(c) and (d)). For the case of NO gas molecule adsorption over C defected α-CN, NO gas molecule behaves as a charge donor whereas for C defected α-CP, behaviour of NO gas molecule of charge acceptor, leads to charge depletion region over α-CP monolayer. (See figure 3.7 (g) and (h)).

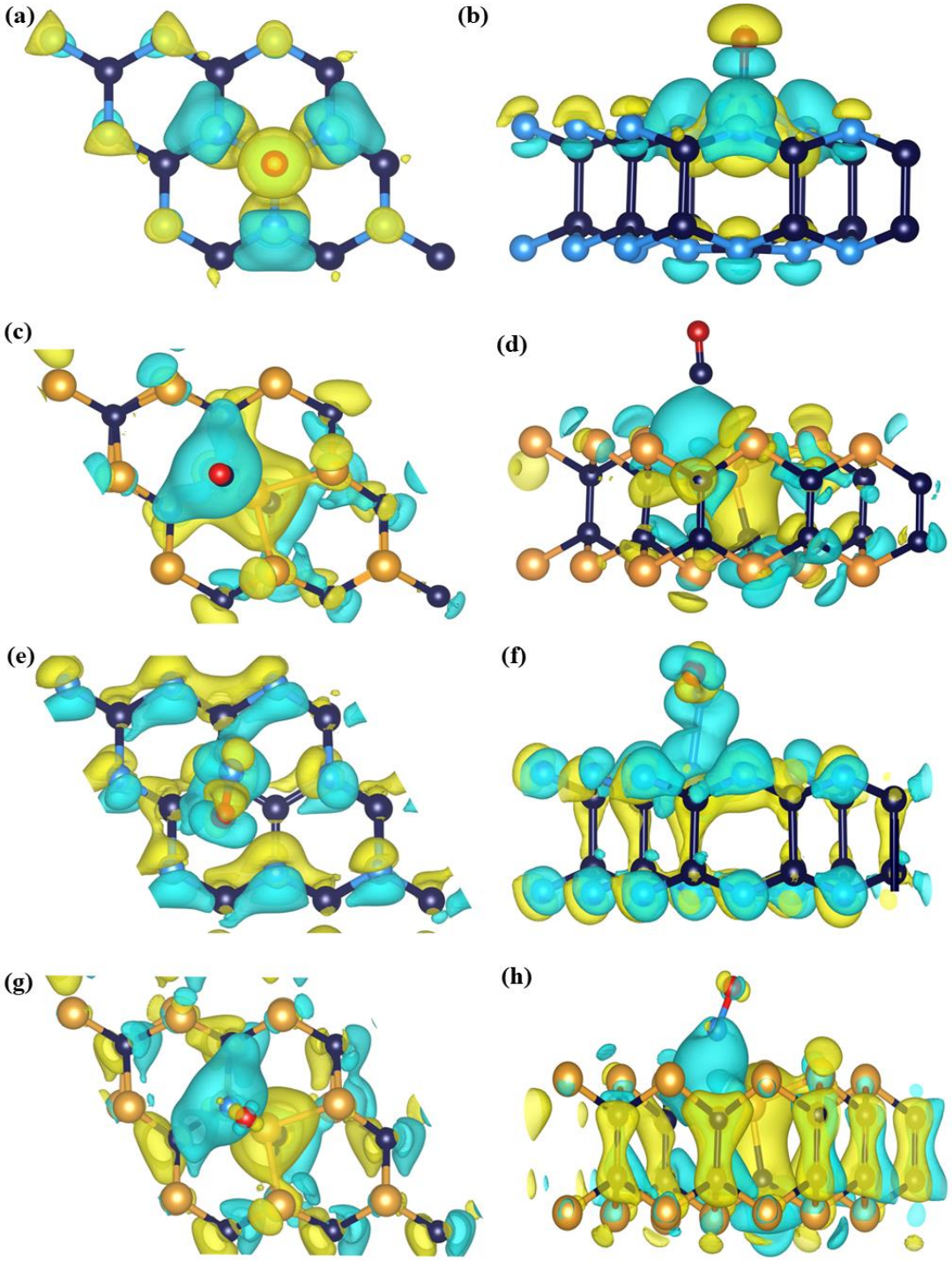

Figure 3.7: Charge density difference plot with (a) Top and (b) side view of C defected α-CN+CO gas; (c) Top and (d) side view of C defected α-CP+CO gas; (e)top and (f) side view of C defected α-CN+NO gas (g) top and (h) side view of α-CP+NO gas.

3.3.5 Work Function

The Fermi level and work function (ϕ) of the material are affected by the gas adsorption; therefore, it is necessary to inspect key components for a ϕ-type sensor. Kelvin oscillator instrument is used in the ϕ-type sensors for the estimation of ϕ-values before and after an adsorption operation for gas molecules. The gate voltage is interrupted when the sensor's work function is increased or decreased by gas adsorption, which produces an electrical signal. The work function (ϕ) is given by the equation below and is defined as the least amount of energy needed to remove one electron from a material to a location in the vacuum immediately outside the solid surface[22].

$$\varphi = V_{el(+\alpha)} - E_F \text{ ----- (3)}$$

where $V_{el(+\alpha)}$ and E_F are electrostatic potential energy far from material surface and Fermi energy respectively. From equation (2), if $V_{el(+\alpha)} = 0$, we can write $\varphi = -E_F$. The variation in the value of φ of an adsorbent system during gas adsorption process changes its field emission characteristics, which can be correlated using a classical Richardson-Dushman equation. The field emission current density for electron in vacuum is given by Richardson-Dushman equation[22]

$$j = AT^2\exp(-\varphi/kT) \text{ ----- (4)}$$

where A stands for Richardson constant (A/m^2) and T is the temperature.

Table 3.4: Work function analysis of α-CN and α-CP monolayers upon CO and NO adsorption

Mono-layer	System	ϕ (before adsorption) (eV)	ϕ (after CO adsorption) (eV)	ϕ (after NO adsorption) (eV)	Δϕ (CO adsorption)	Δϕ (NO adsorption)
α-CN	Pristine	4.89	4.53	5.37	-7.36%	9.81%
	C defected	6.54	4.96	5.74	-24.1%	-12.2%
α-CP	Pristine	5.22	5.25	4.46	0.57%	-14.5%
	C defected	5.21	5.25	5.62	7.87%	0.77%

Equation (4) indicates that the field emission current density is inverse exponentially proportional to the work function. Which implies that the system which has considerable change in ϕ upon adsorption, will make a good candidate for work function based (ϕ- type) sensor. For C-defected α-CN, the most substantial change in work function occurs with CO adsorption, showing a decrease of 24.1%. In contrast, for NO adsorption, the most significant variation in work function is observed in pristine α-CP, with a decrease of 14.5%. Therefore, C-defected α-CN and pristine α-CP are the best candidates for ϕ-type sensors for detecting CO and NO gases, respectively.

3.3.6 Recovery Time Analysis

For gas sensors, the recovery time (τ) is yet another important property. It can be characterised as the projected time till the adsorbate self-desorbs. In other words, recovery time determines how simple or complex the desorption process is[23]. A sensor's recovery time should be faster in the ideal scenario[16]. Strong interactions with gases should be avoided by gas sensors since they make it more difficult for the gas molecules to dissociate and cause the sensor to delay desorption due to the longer recovery time. τ is given by[24]:

$$\tau = \upsilon^{-1} \exp\left(-\frac{E_{ad}}{KT}\right) \text{----- (4)}$$

To calculate τ, we have taken attempt frequency $\upsilon = 10^{12}$ s^{-1} (for IR radiation) and absolute temperature T = 300 K. Table 3.5 shows the recovery time values for pristine and C defected α-CN and α-CP monolayers, in cases of CO and NO adsorption. In the case of CO adsorption, the computed recovery time is longest for C-defected α-CN (1.26×10^{49} s). For the NO adsorption, is the longest for C-defected α-CN as well (1.05×10^{22} s). Pristine α-CN and α-CP for NO adsorption and pristine α-CN for CO adsorption, yield very short recovery times, but they are not suitable candidates for gas sensors owing to their negligible adsorption energies, and large adsorption distances.

Table 3.5: Recovery times for different gas adsorptions

Gas molecule	Monolayer	System	τ (s)
CO	α-CN	Pristine	22.95×10^{-12}
		C-defected	01.26×10^{49}
	α-CP	Pristine	10.58×10^{-12}
		C-defected	02.69×10^{10}
NO	α-CN	Pristine	18.19×10^{-12}
		C-defected	01.05×10^{22}
	α-CP	Pristine	32.51×10^{-12}
		C-defected	02.2610^{21}

3.4 Conclusion

After conducting thorough analysis, it has been determined that neither pristine α-CN nor α-CP yield optimal results for the adsorption of the hazardous CO and NO gases. This is perhaps due to the wide energy band gaps, the adsorption energy values falling within the range of physisorption, and the adsorption distances exceeding 3 Å. To overcome these shortcomings, we have done functionalization of pristine α-CN and α-CP by introducing a defect. Therefore, we have introduced a defect by removing one carbon atom, to amplify the adsorption performance of the pristine α-CX (X = N, P) monolayers. Following the creation of the defect, there has been a significant increase in the adsorption energy value in both cases. In case of functionalized α-CX, the adsorption energy order for CO gas goes as: E (C-defected α-CN) > E (C-defected α-CP). For NO adsorption, the energy order is: E (C-defected α-CP) > E (C-defected α-CN). Which implies that C-defected α-CN is most suitable for CO adsorption. The computed recovery times are extremely long (exceeding several hours) in the best-case scenarios, this implies that C-defected α-CN and C defected α-CP are most suitable for CO and NO gas removal applications.

Bibliography:

1 O. Chamberlain, *Adv. Automob. Eng.*, , DOI:10.4172/2167-7670.1000151.

2 Y. Yamini and M. Moradi, *Sensors Actuators, B Chem.*, 2014, **197**, 274–279.

3 B. Roondhe, K. Patel and P. K. Jha, *Appl. Surf. Sci.*, , DOI:10.1016/j.apsusc.2019.143685.

4 W. Jiang, H. Wang, X. Zhang, Y. Zhu and Y. Xie, *Sci. China Chem.*, 2018, 61, 1205–1213.

5 P. Patel, S. Patel, D. Chodvadiya, M. H. Dalsaniya, D. Kurzydłowski, K. J. Kurzydłowski and P. K. Jha, *J. Energy Storage*, 2023, **71**, 10–13.

6 T. K. Gajaria, D. Chodvadiya and P. K. Jha, *ACS Appl. Nano Mater.*, 2021, **4**, 4474–4483.

7 S. Yang, C. Jiang and S. huai Wei, *Appl. Phys. Rev.*, 2017, 4.

8 H. Mistry, D. Chodvadiya, S. Vadalkar, K. N. Vyas and P. K. Jha, *Surfaces and Interfaces*, 2024, 46.

9 Y.-H. Zhang, Y.-B. Chen, K.-G. Zhou, C.-H. Liu, J. Zeng, H.-L. Zhang and Y. Peng, *Nanotechnology*, 2009, **20**, 185504.

10 M. Ghambarian, Z. Azizi and M. Ghashghaee, *Chem. Eng. J.*, 2020, **396**, 125247.

11 Y. Gao, S. Liu, W. Chen, J. Yu, L. Wang and P. Li, *Mater. Sci. Semicond. Process.*, 2024, **179**, 3–6.

12 W. Kohn, A. D. Becke and R. G. Parr, *Density Functional Theory of Electronic Structure*, 1996.

13 P. Giannozzi, S. Baroni, N. Bonini, M. Calandra, R. Car, C. Cavazzoni, D. Ceresoli, G. L. Chiarotti, M. Cococcioni, I. Dabo, A. Dal Corso, S. De Gironcoli, S. Fabris, G. Fratesi, R. Gebauer, U. Gerstmann, C. Gougoussis, A. Kokalj, M. Lazzeri, L. Martin-Samos, N. Marzari, F. Mauri, R. Mazzarello, S. Paolini, A. Pasquarello, L. Paulatto, C. Sbraccia, S. Scandolo, G. Sclauzero, A. P. Seitsonen, A. Smogunov, P. Umari and R. M. Wentzcovitch, *J. Phys. Condens. Matter*, 2009, **21**, 44.

14 J. P. Perdew and K. Burke, *Phys. Rev. B - Condens. Matter Mater. Phys.*, 1996, **54**, 16533–16539.

15 J. D. Pack and H. J. Monkhorst, *Phys. Rev. B*, 1977, **16**, 1748–1949.

16 S. Kanti Jana, N. N. Som and P. K. Jha, *J. Mol. Liq.*, 2023, **383**, 1–4.

17 D. Chodvadiya, S. B. Pillai, B. Chakraborty and P. K. Jha, in *AIP Conference Proceedings*, American Institute of Physics Inc., 2020, vol. 2265.

18 S. Vadalkar, D. Chodvadiya, N. N. Som, K. N. Vyas, P. K. Jha and B. Chakraborty, *ChemistrySelect*, 2022, **7**, e202103874.

19 R. K. Choudhury, B. R. Bhagat, K. H. Mali, R. Pokar and A. Dashora, *Appl. Surf. Sci.*, , DOI:10.1016/j.apsusc.2022.154426.

20 D. Chodvadiya, N. N. Som, P. K. Jha and B. Chakraborty, *Int. J. Hydrogen Energy*, 2021, **46**, 22478–22498.

21 D. Chodvadiya, S. Kanabar, B. Chakraborty and P. K. Jha, *Int. J. Hydrogen Energy*, 2024, **53**, 958–968.

22 Y. Liu, C. Liu and A. Kumar, *Mol. Phys.*, , DOI:10.1080/00268976.2020.1798528.

23 A. Yadav, *Comput. Theor. Chem.*, , DOI:10.1016/j.comptc.2022.114005.

24 S. Vadalkar, D. Chodvadiya, K. N. Vyas and P. K. Jha, *Mater. Today Proc.*, 2022, **67**, 229–237.